UCSF

UC San Francisco Previously Published Works

Title

A Lipid E-MAP Identifies Ubx2 as a Critical Regulator of Lipid Saturation and Lipid Bilayer Stress

Permalink

Journal

ISSN

Authors

Surma, Michal A
Klose, Christian
Peng, Debby
et al.

Publication Date

DOI

Peer reviewed

A Lipid E-MAP Identifies Ubx2 as a Critical Regulator of Lipid Saturation and Lipid Bilayer Stress

Michal A. Surma[1,2], **Christian Klose**[1], **Debby Peng**[2], **Michael Shales**[2], **Caroline Mrejen**[4], **Adam Stefanko**[5], **Hannes Braberg**[2], **David E. Gordon**[2], **Daniela Vorkel**[1], **Christer S. Ejsing**[5], **Robert Farese Jr.**[3,4], **Kai Simons**[1], **Nevan J. Krogan**[2,4,*], and **Robert Ernst**[1,6,*]

[1]Max Planck Institute of Molecular Cell Biology and Genetics, 01307 Dresden, Germany

[2]Department of Cellular and Molecular Pharmacology, California Institute for Quantitative Biosciences

[3]Departments of Medicine and Biochemistry & Biophysics University of California, San Francisco, San Francisco, CA 94158, USA

[4]Gladstone Institute of Cardiovascular Disease, San Francisco, CA 94158, USA

[5]Department of Biochemistry and Molecular Biology, University of Southern Denmark, 5230 Odense, Denmark

[6]Goethe University Frankfurt, Institute of Biochemistry, 60438 Frankfurt, Germany

SUMMARY

Biological membranes are complex, and the mechanisms underlying their homeostasis are incompletely understood. Here, we present a quantitative genetic interaction map (E-MAP) focused on various aspects of lipid biology, including lipid metabolism, sorting, and trafficking. This E-MAP contains ~250,000 negative and positive genetic interaction scores and identifies a molecular crosstalk of protein quality control pathways with lipid bilayer homeostasis. Ubx2p, a component of the endoplasmic-reticulum-associated degradation pathway, surfaces as a key upstream regulator of the essential fatty acid (FA) desaturase Ole1p. Loss of Ubx2p affects the transcriptional control of *OLE1*, resulting in impaired FA desaturation and a severe shift toward more saturated membrane lipids. Both the induction of the unfolded protein response and aberrant nuclear membrane morphologies observed in cells lacking *UBX2* are suppressed by the supplementation of unsaturated FAs. Our results point toward the existence of dedicated bilayer stress responses for membrane homeostasis.

INTRODUCTION

The biological membrane is a defining feature of all cellular life forms. Cell membranes possess a staggering complexity of lipids and proteins that cooperate for the compartmentalization of biochemical processes and allow for the selective exchange of molecules and information (van Meer et al., 2008). Lipids play a central role in shaping the physicochemical environment of the membrane, which, in turn, affects the membrane proteins (Phillips et al., 2009). The molecular packing of lipids is the underlying principle of phase behavior and membrane fluidity. Cellular lipids exhibit a large fraction of kinked and

"poorly" packed unsaturated fatty acids (UFAs) for increasing the fluidity of the membrane at physiological temperatures (van Meer et al., 2008). Generally, saturated fatty acid (SFA)-containing lipids can pack with a higher order and have higher melting temperatures. Not surprisingly, lipid saturation is subject to crucial regulation in response to changes of temperature and other conditions for cellular growth (Klose et al., 2012).

Membrane proteins evolved with the surrounding membrane lipids to achieve optimal biological activity, but they also contribute to the general structural properties of biological membranes (Kaiser et al., 2011). Systematic interrogations of cellular pathways elucidated a crosstalk between lipid metabolism and protein quality control systems, such as the unfolded protein response (UPR) and the endoplasmic reticulum (ER)-associated degradation (ERAD) pathway, which is responsible for removing aberrant proteins from the ER (Jonikas et al., 2009; Schuldiner et al., 2005). These findings have placed fresh emphasis on the regulation of lipid metabolism and provided a different perspective to the field of protein homeostasis. An important role of fatty acids (FAs) in cellular stress responses has been recognized in both *Saccharomyces cerevisiae* and mammals (Eizirik and Cnop, 2010; Kohlwein and Petschnigg, 2007). A misbalance between SFAs and UFAs in the diet and, consequently, cells induces ER stress and can lead to cell death (Kim et al., 2008). Conversely, a massive induction of ER stress is counterbalanced by the increased utilization of FAs for lipid synthesis and expansion of the ER (Bernales et al., 2006; Schuck et al., 2009). This introduces a conundrum surrounding the nature by which ER stress is modulated by lipid species.

Functional relationships between the different cellular processes involving lipids and other factors might be uncovered through genetic interaction mapping of the genes of interest. Genetic interactions have been employed for decades in order to evaluate the functional relationships of genes by identifying synthetic sickness and/or lethality. More recently, this type of analysis achieved a higher level of predictive power with the development of epistatic miniarray profiles (E-MAPs) (Roguev et al., 2008; Schuldiner et al., 2005). Here, a large set of double mutants is generated, and the growth of these double mutants is measured according to colony size. Both negative (aggravating) and positive (alleviating) pairwise epistatic relationships between genes are determined and expressed quantitatively as S-scores by calculating the deviations of the observed growth rate of each double mutant from the expected growth rate in the absence of a genetic interaction. Negative genetic interactions occur if a double mutant is less fit than expected (synthetic sickness and /or lethality), whereas positive genetic interactions occur if a double mutant is fitter than expected (alleviation). The frequency of strong genetic interactions between randomly chosen genes is low, but this frequency is much higher for functionally related genes.

Using E-MAP data, functional groups of genes can be identified through the unbiased hierarchical clustering of genetic interaction profiles, but patterns of interactions with all other genes in the study can also be used to gain insight into gene functions (Beltrao et al., 2010). E-MAPs have proven to be a powerful technique for discovering gene functions, identifying structural complexes, and organizing them into pathways (Aguilar et al., 2010; Collins et al., 2007b; Hoppins et al., 2011; Schuldiner et al., 2005).

Here, we present an E-MAP focused on *S. cerevisiae* genes involved in lipid metabolism, sorting, post-Golgi trafficking, and related processes that complements previous E-MAPs that focused on the early secretory pathway, the plasma membrane, and endocytosis (Aguilar et al., 2010; Schuldiner et al., 2005). Combined with quantitative lipidomics, we uncover an intriguing connection between FA desaturation, the UPR, and ERAD machinery. Ubx2, a central component of the ERAD pathway (Neuber et al., 2005; Schuberth and Buchberger, 2005), emerges as a key upstream regulator of the single, essential FA

desaturase of *S. cerevisiae* Ole1 (Stukey et al., 1990). Our results identify a molecular link between protein degradation and FA desaturation and reveal insight into the regulation of membrane homeostasis.

RESULTS

Generation of a Lipid E-MAP

To study the interconnections of lipid metabolism and protein homeostasis, we used a quantitative genetic interaction map, or E-MAP, to functionally interrogate a set of 741 genes (corresponding to ~13% of the *S. cerevisiae* genome), 133 of which were essential (Table S1 available online). The genes, selected on the basis of Gene Ontology terms, represent several functional categories, including the trafficking and metabolism of lipids (Figure 1A). In total, we identified 251,383 genetic interactions (see Data S2). As a quality control, we checked the correlation between replicate measurements where the query and array strains were flipped (i.e., A-B versus B-A), which provided a strict test, given that such flipped replicates originate from independently created double mutants. Our replicate genetic scores are highly correlated (r = 0.661) (Figure 1B), more so than those of other data sets that have been generated (Collins et al., 2007b; Costanzo et al., 2010; Schuldiner et al., 2005; Wilmes et al., 2008), implying a genetic interaction map of high quality (Figure S1A). Nevertheless, the measured interactions are highly correlated with these previous studies (Figure S1B) without being redundant. Out of the entire data set, ~50% of the interactions (134,059) have not been measured in previous screens (Figure 1C).

Our results are consistent with previous reports of a correlation between physically associated proteins and the corresponding genes displaying similar interaction profiles (Collins et al., 2007b) (Figure S1C). With a set of 90 high-confidence protein-protein interactions (PPIs) (Table S2) (Babu et al., 2012; Collins et al., 2007a), we compared the correlation of genetic profiles of the corresponding genes from this E-MAP and from a larger screen (Costanzo et al., 2010). Even though our E-MAP covers only 741 genes in comparison to the larger screen, covering several thousand genes, almost all the profiles from the PPI pairs are more highly correlated within our data set (Figures 1D and S1D), again implying a high-quality genetic interaction data set.

Hierarchical clustering of the correlation coefficients of genetic interaction profiles recapitulates known pathways and complexes and identifies previously unrecognized connections (Figure 1E and Data S1). For example, we identified clusters of genes involved in ER protein folding and -1-6-glucan synthesis, vacuolar delivery, and peroxisome function. Interestingly, the sphingolipid biosynthesis cluster, which includes *TSC10*, *TSC13*, and *PHS1*, also contains a component of a chromatin structure remodeling complex (*RSC3*) (Lorch et al., 1998), thereby suggesting a link between chromatin biology and sphingolipid metabolism.

This wealth of genetic interaction data on diverse aspects of cell biology with many more evident connections can be harnessed for in-depth interrogation and rigorous biochemical characterization (Supplemental Information).

Uncovering Potential Regulators of Phosphatidylcholine Synthesis

Our lipid E-MAP uncovered candidates for the regulation of the well-characterized pathways of phosphatidylcholine (PC) biosynthesis. The data set includes genes involved in the two parallel branches of PC synthesis (*PSD1*, *CHO2*, and *OPI3* [phosphatidylserine (PS) to PC conversion pathway] and *PCT1*, *CKI1*, and *CPT1* [Kennedy pathway]) whose genetic interaction profiles clustered separately (Figure 2B) and showed strong negative interactions between gene pairs both within and across branches (Figure 2C). Negative interactions

between genes from two branches of a biochemical pathway result from both branches contributing to the same pool of critically important products—in this case, PC species.

SNF4 encodes a subunit of AMP-activated Snf1 kinase complexes, which are critical for gene regulation in response to glucose but have not been implicated in the modulation of PC synthesis. An inspection of the clustered E-MAP data identified highly negative interaction scores and clustering of *SNF4* with genes from the PS to PC (Figure 2C), but not the Kennedy (Figure 2C), pathway. Because yeast lipidomes are remodeled in response to glucose (Klose et al., 2010), these data specifically implicated *SNF4* in the regulation of PS to PC conversion, suggesting a link between glucose sensing and glycerolphospholipid synthesis by a mechanism that is yet to be characterized.

Similarly, our data connect the triacylglycerol lipase encoded by the *TGL2* gene with the Kennedy pathway, given that *TGL2* specifically clustered with Kennedy pathway genes (Figure 2B). Moreover, *TGL2* exhibited highly negative genetic interactions with *CHO2* and *OPI3*, the genes from the other branch, which is typical for parallel pathways (Figure 2C). Given that diacylglyceroles (DAGs) are the products of Tgl2 and that DAGs are required for the Kennedy pathway, it is likely that Tgl2 serves as a DAG donor for PC synthesis. Additional triacylglycerol lipase-encoding genes, such as *TGL1*, *TGL3*, and *TGL4*, did not show similar genetic interactions, suggesting a specific function of Tgl2 for the Kennedy pathway. This interpretation is substantiated by the subcellular localization of these enzymes; Tgl2 and Cpt1 (the next-in-pathway enzyme) localize to mitochondria, whereas Tgl1, Tgl3, and Tgl4 localize to different organelles (Henry et al., 2012). Altogether, our analysis suggests that Tgl2 generates DAG for the de novo synthesis of PC. These examples of *SNF4* and *TGL2* illustrate the potential of this E-MAP to identify or implicate genes in specific cellular pathways.

Genetic Interaction between Protein Degradation and FA Desaturation

Our E-MAP highlighted an intricate connection between the protein quality control machinery and FA desaturation. Specifically, we found a strong negative genetic interaction between the *UBX2* gene, which encodes a component of the ERAD pathway (Neuber et al., 2005), and *OLE1*, the single and essential FA desaturase gene of *S. cerevisiae* (Figures 2D–2F). In the same network of genetic interactions, we also found *MGA2* and *SPT23*, which encode two transcriptional regulators that cooperatively mediate and modulate the expression of *OLE1* (Figure 2F) (Kandasamy et al., 2004). These regulators are ER membrane proteins and have to be activated in order to drive *OLE1* transcription (Figure 2G). To this end, Mga2 and Spt23 become ubiquitylated and processed by the action of the proteasome and the Cdc48 ATPase along with its ubiquitin-binding cofactors Npl4 and Ufd1 (Hoppe et al., 2000; Rape et al., 2001; Shcherbik and Haines, 2007). Partial degradation of the membrane-embedded precursor (P120) releases a soluble and active transcriptional activator (P90) from the ER that translocates to the nucleus in order to drive the expression of *OLE1* (Figure 2G).

The OLE pathway shares several similarities and components with the ERAD pathway, wherein Ubx2 acts as a membrane anchor for Cdc48 and recruits ubiquitylated, misfolded proteins to their site of membrane extraction (Neuber et al., 2005). Therefore, a strong genetic interaction of *UBX2* with the UPR components *IRE1* and *HAC1* was not surprising (Ron and Walter, 2007) (Figures 2E and 2F). However, our genetic data imply an equally important function of Ubx2 for the modulation of FA desaturation, and the pronounced negative genetic interactions of *UBX2* with *SPT23* and *OLE1* led us to question to what extent *UBX2* contributes to FA metabolism and membrane biogenesis (Figures 2D–2F).

We directly tested a role of *UBX2* in *OLE1* expression and the regulation of the Ole1 level (Figures 2H and 2I). Growing *ubx2* and *mga2* cells exhibited a reduced messenger RNA (mRNA) level of *OLE1* (Figure 2H), resulting in a 40% and 50% drop of the Ole1 enzyme level in comparison to wild-type (WT) cells (Figure 2I). Although a reduction by a factor of two may appear modest, one should bear in mind that *OLE1* is an essential gene and that its products, UFAs, are abundant building blocks for membrane biogenesis.

The Lipid Composition of a Desaturase-Depleted Cell

We employed quantitative mass-spectrometry-based shotgun lipidomics to study the impact of a reduced Ole1 level on the membrane lipid composition (Ejsing et al., 2009). The lipidomes of *ubx2* or *mga2* cells were strikingly different from WT controls (Figures 3A–3C and S2). In *ubx2* cells, we observed a systematic shift toward more saturated lipids manifested by a dramatic increase of glycerophospholipids with two saturated acyl chains (double bonds [DB] = 0) at the expense of glycerophospholipids with two monounsaturated acyl chains (DB = 2). This effect was even more pronounced in *mga2* cells but unexpectedly absent in *spt23* cells (Figure 3A). An increased fraction of saturated lipids was observed with varying degree in all glycerolphospholipid classes (Figures 3B and S3). The effect was remarkably specific and was not phenocopied by the deletion of *HRD1* or *DOA10*, the two major E3 ubiquitin ligases of the ERAD system (Vembar and Brodsky, 2008) or by the deletion of other UBX-domain-encoding genes (*UBX3* to *UBX7*) (Figure S4). This is noteworthy because of the overlapping functions of Ubx2 and Ubx4 in the ERAD pathway (Alberts et al., 2009) and because the tested UBX domain containing proteins exert their diverse cellular functions via a common mechanism: the recruitment of ubiquitylated substrates to the abundant ATPase Cdc48 (Schuberth and Buchberger, 2008). Our data identify a specific function of Ubx2 and illustrate the remarkable modularity of the ERAD system.

Cellular Adaptations to Perturbed FA Metabolism Caused by *UBX2* Deletion

Saturated and tightly packing glycerophospholipids have a major impact on the biophysical properties of a membrane. How does a cell cope with a highly increased fraction of saturated acyl moieties? In comparison to WT cells, *ubx2* cells displayed significant changes in virtually all lipid classes (Figure 3C and Table S3), which may partly compensate for the severe changes in the FA composition. Even the levels of ergosterol and sphingolipids (MIPC and MIP_2C) were significantly perturbed, although these lipids did not incorporate UFAs, suggesting widespread homeostatic effects. Notably, the increased abundance of lipids with relatively small head groups, such as PA and PE at the expense of PC, could compensate for the intrinsic curvature stress imposed by the reduced volume occupied by the saturated acyl chains in the hydrophobic core of the membrane (Figure 3C). Thus, the shift toward more saturated membrane lipids in *ubx2* cells is accompanied by major rearrangements in lipid classes for maintaining membrane shape and fluidity.

A Complex Interplay of Regulatory Factors Determines the Level of Ole1

Membrane homeostasis requires a tight regulation of the Ole1 level. Because we assessed the level of Ole1 expressed from its endogenous locus and promoter, we could identify Mga2 as the dominant factor determining the desaturase level in exponentially growing cells (Figure 2I). Surprisingly, the lack of Spt23, the other transcriptional regulator, did not interfere with the expression of *OLE1* as efficiently as the loss of Mga2 or Ubx2 and barely affected the resulting desaturase level (Figures 2H and 2I). Spt23 can compensate for the lack of Ubx2 or Mga2 when cells resume growth from the stationary phase, but, upon increased demand for de novo lipid synthesis, Ubx2 and Mga2 become critical for yielding high levels of Ole1 (Figure S5).

As a feedback control, excess dietary UFAs abrogate the expression of *OLE1* and destabilize the mRNA of *OLE1* (Kandasamy et al., 2004). In the presence of dietary linoleate (18:2), the *OLE1* mRNA level dropped significantly in WT and *ubx2*, *mga2*, and *spt23* cells (Figure 4A). Thus, none of these three genes encodes the sole sensor for the regulation of the OLE pathway. Consistent with the UFA-induced drop of mRNA abundance, the Ole1 enzyme level was markedly reduced in the presence of linoleate (18:2) in WT cells (Figure 4B). Intriguingly, the dynamic range of this response was dampened in *ubx2* cells, implying that a posttranslational mechanism might also be at work. We conclude that Ubx2 is required for normal *OLE1* expression and that Mga2 is the dominant factor controlling the mRNA level of *OLE1* in growing cells.

The processing and activation of Spt23 and Mga2 via the OLE pathway (Figure 2G) shares components and mechanistic cues with the ERAD pathway. Because Cdc48 and its ubiquitin-binding cofactors Ufd1 and Npl4 have been shown to release active P90 fragments of Spt23 and Mga2 from the ER membrane (Rape et al., 2001; Shcherbik and Haines, 2007) and Cdc48-Ufd1-Npl4 has been implicated in processing in Spt23 (Hitchcock et al., 2001), we were interested whether Ubx2 might assist this reaction. In *ubx2* cells, we observed the accumulation of the membrane-embedded full-length Spt23 P120 as ubiquitylated species and a mildly reduced level of Spt23 P90 (Figures 4C and 4D), suggesting a processing defect. No accumulation of P120 was observed in cells lacking one of the two central E3 ubiquitin ligases of the ERAD system (Hrd1/Der3 and Doa10) or Ubx4 (Vembar and Brodsky, 2008). A complex of Spt23 and Ubx2 was detectable only when downstream events were blocked by the temperature-sensitive *cdc48-3* mutation, implying a very transient interaction in WT cells (data not shown). Along with our lipidomic survey of several UBX-domain-containing proteins (Figure S4), the processing of Spt23 reveals a specific function of Ubx2 in the regulation of *OLE1* expression and, consequently, membrane lipid saturation.

Stationary cells that do not depend on de novo lipid biosynthesis stalled the processing of Spt23 into the active P90 form (Figure 4E). When stationary cells resumed growth, they rapidly produced P90, and this was controlled by exogenous UFAs (Figure 4E). In *ubx2* cells, however, the processing of Spt23 was significantly impaired, thereby limiting the response to exogenous UFAs (Figure 4E). Consistent with earlier findings, the Rsp5-dependent ubiquitylation of Spt23 observed in *ubx2* cells was blocked by exogenous linoleate, but less so by oleate (Hoppe et al., 2000) (Figures 4E and S5B), implying that the ubiquitylation reaction per se or an upstream event is responsible for stalling the activation of Spt23 in the presence of abundant UFAs.

Examination of Mga2, the dominant regulator of mRNA abundance, revealed an increased level of both P120 and processed P90 Mga2 in *ubx2* cells, suggesting a role of *UBX2* in controlling the steady state level, but not for the processing reaction, of Mga2 (Figure 4F). In contrast to Spt23, proteolytic processing of Mga2 is independent of ubiquitylation by Rsp5 (Shcherbik et al., 2003) and, consequently, does not seem to require Ubx2 (Figure 4F). Nevertheless, our experiments provide compelling evidence that Ubx2 affects the Ole1 enzyme level via both Spt23 and Mga2.

Like Hmg2, a key enzyme for sterol production, Ole1 is intrinsically unstable and processed via the ERAD pathway (Bays et al., 2001; Braun et al., 2002). When Ole1 was expressed from a *GAL* promoter, the steady-state level was increased in cells lacking central ERAD components such as *UBX2* or the ubiquitin ligase *HRD1/DER3* (Figure 4G) (Bordallo et al., 1998; Hampton et al., 1996). Supporting this, immunoprecipitation (IP) experiments identified a physical interaction of both Ubx2 and Ole1 with the ERAD-specific ubiquitin ligase Hrd1/Der3, all of which were expressed at their endogenous levels (Figure 4H). We

conclude that Ole1 is degraded by the ERAD system in an Ubx2-dependent manner and that Ubx2 does not only regulate the level of Ole1 by modulating transcription via Mga2 and Spt23.

UPR Induction in Cells with Membrane Lipid Alternations Due to the Deficiency of *UBX2* or *MGA2*

The accumulation of misfolded proteins in the lumen of the ER activates the UPR (Ron and Walter, 2007), but perturbations with lipid metabolism can also induce UPR signaling (Han et al., 2010; Kohlwein and Petschnigg, 2007; Pineau et al., 2009; Volmer et al., 2013). We wondered whether lipidome remodeling as observed for *ubx2* and *mga2* cells resulted in cellular stress. We adapted a fluorescence-activated cell sorting (FACS)-based assay by Jonikas et al. (2009) to score for UPR activation by driving the expression of GFP from a promoter with four repeats of the unfolded protein response element. We validated the assay by titrating WT cells with dithiothreitol (DTT), a drug interfering with protein maturation in the ER (Figure 5A). Our experiments confirmed that *mga2* and *ubx2* cells exhibit a strong activation of the UPR (Figure 5B). Because of its critical role in FA desaturation and because lipid saturation might directly contribute to UPR signaling (Volmer et al., 2013), we tested a causative role of the FA composition by supplementation with UFAs. Although WT and *hrd1/der3* cells were mildly stressed by oleate, the strong activation of the UPR in *ubx2* and *mga2* cells was greatly relieved by UFA feeding (Figure 5B). The lipidomic analysis of WT and *ubx2* cells grown with oleate showed an indistinguishable yet higher degree of UFA incorporation in membrane and storage lipids (Figures 5C and 5D). Likewise, almost all differences in the lipid class profile of WT versus *ubx2* cells (Figure 3C) were abolished upon UFA feeding (Figure 5E). Exogenous oleate overcompensated the limited ability of *ubx2* cells to mediate high-level expression of Ole1 and the resulting deficit of UFAs. This reversible change of the lipid class composition suggested that the lipidome change in *ubx2* cells represented a direct consequence of perturbed FA desaturation, an active adaptation, or both.

Membrane Whorls of the Outer Nuclear Membrane Due to the Deficiency of *UBX2* or *MGA2*

The increased level of saturated lipids in *mga2* and *ubx2* cells, as well as the activation of the UPR under UFA-limiting conditions, prompted us to investigate the cellular anatomy of these mutants by electron microscopy. In contrast to the normal nuclear morphology observed in WT cells (Figures 6A and 6D), we frequently observed whorl formation of the outer nuclear membrane in *ubx2* and *mga2* cells (Figures 6B, 6C, and 6E–6G). Similar aberrant morphologies were observed in 70 nm sections in more than 10% of *ubx2* and 30% of *mga2* cells, and their size ranged from 100–600 nm (Figures 6F and 6G). We also observed a putatively early stage of whorl formation where the outer nuclear membrane only protruded from the nucleus (Figure 6E). To establish whether the reduced degree of FA desaturation observed in *ubx2* and *mga2* was causative for membrane proliferation and whorl formation, we grew cells in the presence of oleate (Figures 6H–6J). Not a single whorl was observed under these conditions, but an increased content of lipid droplets as a consequence of oleate-induced triacylglyceride (TAG) synthesis was observed (Hapala et al., 2011) (Figure 5E). Whorls were also observed in a *ubx2 mga2* mutant (Figure 6K).

Like DTT-treated cells, *ubx2* and *mga2* cells exhibit a strong activation of the UPR (Figure 5B). However, although DTT-induced stress resulted in the proliferation of the cortical ER (Figure 6L) (Bernales et al., 2006), cells stressed by an overly saturated lipid composition expanded their outer nuclear membrane into whorls. Because DTT acts in the lumen of the ER but the deletion of *UBX2* or *MGA2* affects the ER membrane composition, we speculate that the nature and the origin of ER stress might determine the site of ER expansion.

Finally, we examined whether the formation of whorls in cells with augmented FA desaturation was solely driven by the lipid composition or whether it might represent an active cellular process. We blocked the signal propagation of the UPR by deleting *HAC1* to test whether UPR signaling was required for whorl formation (Ron and Walter, 2007). Given that *ubx2 hac1* cells are not viable, we inspected *mga2 hac1* cells. Although *mga2 hac1* cells exhibited characteristic lipidome changes similar to those observed in *ubx2* and *mga2* cells (Figure S6), we could not find a single whorl in these cells (Figure 6M). Therefore, whorl formation represents an active process that requires a functional UPR.

DISCUSSION

Here, we present a genetic interaction map focused on lipid biology and post-Golgi trafficking. This data set is accessible for browsing (Data S2), reveals connections between cellular machineries and pathways that can be used to infer future directions of research, and identifies putative regulators of PC synthesis. From the wealth of data obtained, we focused on the function of Ubx2; i.e., linking protein homeostasis to lipid metabolism.

Given that the ER is the organelle of membrane protein insertion and a major site for lipid biosynthesis, one may expect that the components of the ER membrane and its lipids, and proteins are co-regulated. We show that Ubx2 is a fundamental component of this connection. Its dual role in the ERAD and OLE pathways physically links these processes and emphasizes a structure-function relationship through which ER bioactivity is regulated.

Modes of UFA Synthesis Regulation

Cells require UFAs for lipid synthesis, and the resulting membrane properties are influenced by the fraction of saturated lipids. Therefore, the level of Ole1 is regulated by several mechanisms (Martin et al., 2007). Ubx2 affects the level of Ole1 substantially by three distinct ways: via Mga2, via Spt23, and by mediating the degradation of Ole1. Our data are consistent with Ubx2 acting as a substrate-recruiting factor by guiding Mga2 and Spt23 to Cdc48, which releases the soluble P90 fragments from the ER membrane (Rape et al., 2001; Shcherbik and Haines, 2007). This function of Ubx2 would be analogous to its role in the ERAD pathway (Vembar and Brodsky, 2008). Remarkably, despite the fact that Ubx7 resides in the same membrane and also binds Cdc48 (Goder et al., 2008), it cannot compensate for the loss of Ubx2. Likewise, the Ubx4 implicated in ERAD and the binding of Cdc48 (Alberts et al., 2009) is not involved in the activation of the OLE pathway.

The role of Ubx2 in assisting the detachment of the transcriptional activators from the ER membrane is tantalizingly simple but might not represent the whole story. We show that Mga2, not Spt23, is the dominant factor controlling the Ole1 level, but we were puzzled by the observation that both a loss of and an increase in Mga2 (as observed in *ubx2* cells) resulted in reduced levels of Ole1p. Mga2, in contrast to Spt23, has a function beyond transcriptional activation; i.e., stabilizing and destabilizing *OLE1* mRNA (Kandasamy et al., 2004). A soluble expressed P90 fragment of Mga2 could only stabilize, but not destabilize, the *OLE1* mRNA, suggesting that this function required the membrane-tethered form of Mga2 (Kandasamy et al., 2004). Therefore, the increase of membrane-associated Mga2 observed in *ubx2* cells might destabilize the *OLE1* mRNA and, thus, decrease the Ole1 level in this mutant. The complex pattern by which Ubx2 modulates *OLE1* expression and the resulting enzyme level illustrates interwoven and interdependent relationships between lipid metabolism and proteostasis.

Intrinsic Mechanisms of Lipid Bilayer Quality Control

The biophysical properties of a membrane are a consequence of the membrane composition. A systematic shift toward more saturated lipids would result in a marked change of the intrinsic membrane curvature because the hydrophobic part of fully saturated lipids occupies a smaller volume than lipids with one or two unsaturated acyl chains. Our lipidomic data reveal that *ubx2* and *mga2* cells exhibit an increased abundance of lipids with relatively small head groups, suggesting a mechanism that enables yeast to counteract intrinsic curvature stress and aberrant lipid packing by modulating the quantities of geometrically different lipid classes (Deguil et al., 2011). This type of regulation represents a reverse scenario to the adaptations observed in PC-depleted cells, which undergo intense acyl chain remodeling (Boumann et al., 2006) and a membrane stress response (Thibault et al., 2012).

A recent study identified a role of Ubx2p for TAG metabolism, lipid droplet size, and composition (Wang and Lee, 2012). Because SFAs are generally less efficiently incorporated into TAGs in comparison to UFAs (Hapala et al., 2011), the decreased abundance of TAGs in *ubx2* cells might reflect the consequence of decreased FA desaturation that is counteracted by exogenous UFAs (Figure 5E). The fact that the reduced TAG levels in *ubx2* cells were restored by the expression of its mammalian homolog Ubxd8 suggests a conserved function of *UBX2*/Ubxd8 for protein degradation and lipid metabolism from yeast to mammals (Wang and Lee, 2012). Intriguingly, Ubxd8, the mammalian homolog of Ubx2, has been proposed to act as an FA sensor and was implicated in the regulation of sterols by acting on Insig1, allowing a cell to coordinate FA utilization and sterol biosynthesis (Lee et al., 2010). At the same time, Ubxd8 is involved in the regulation of lipid droplet turnover by acting on ATGL, the rate-limiting enzyme for lipolysis (Olzmann et al., 2013). Our results exclude the possibility that Ubx2 acts as the sole sensor of the OLE pathway. Cells deleted for *UBX2* readily attenuated *OLE1* expression in the presence of dietary UFAs (Figure 4A). Apparently, interconnected regulatory circuits and more than one sensor evolved to maintain membrane composition and functionality.

Lipid Bilayer Quality Control by the UPR

The UPR controls the secretory capacity of a cell (Ron and Walter, 2007). To this end, the UPR reconfigures protein and lipid synthesis, protein folding, and quality control pathways. The binding mode of ER-lumenal misfolded proteins to Ire1 is established at the molecular level, but the question of how Ire1 senses membrane aberrancies remains enigmatic (Volmer et al., 2013). Truncation mutants of Ire1 lacking the binding domain for misfolded proteins are still modulated by lipids (Promlek et al., 2011). How do perturbations of lipid metabolism such as PC synthesis (Thibault et al., 2011) or sphingolipids induce the UPR (Han et al., 2010)? Consistent with a recent report on the mammalian UPR components IRE1 and PERK (Volmer et al., 2013), we show that an increase of saturated membrane lipids massively induced the UPR. Cells deleted for *UBX2* or *MGA2*, which we know to exhibit aberrant FA desaturation, were found among the top UPR-inducing mutants in a screen by Jonikas et al. (2009). Intriguingly, we show that the high level of UPR activation can be reversed by exogenous UFAs (Figure 5B). This drastic dependence of the UPR on lipid composition can be explained by the molar predominance of lipids in the ER membrane, but the molecular mechanism by which lipids induce the UPR remains to be studied in further detail (Volmer et al., 2013). Only the functional reconstitution of full-length Ire1 in defined membrane environments can reveal the molecular signal(s) underlying the membrane-dependent activation of the UPR.

Whorl Formation of the Nuclear Envelope in Desaturase-Deficient Cells

The ER membrane is an architecturally plastic organelle. It forms a structure of two domains, the outer nuclear membrane, which is a part of the nuclear envelope (NE), and the peripheral ER. The ER can exhibit diverse morphologies; i.e., tubes, sheets, stacks, hexagonal shapes, and whorled ER in concentric or sinusoidal arrangements (Snapp et al., 2003; Voeltz et al., 2002). Such organized smooth ER structures can be induced, for example, by membrane protein overexpression or viral infection. We demonstrated that a shortage of FA desaturation induces the formation of sinusoidal deformations (whorls) of the perinuclear ER, but not of the peripheral ER. In contrast, other types of ER stress induced by tunicamycin or DTT induce a proliferation of the peripheral ER, but not the NE (Bernales et al., 2006). The nature and origin of stress seems to determine the cellular localization of membrane deformations.

The full reversal of whorls by UFA supplementation establishes a causative role of lipids for their formation, but, clearly, an increased fraction of saturated lipids is not sufficient for ER whorl formation. Instead, the sinusoidal proliferation of the perinuclear ER represents an active cellular process that requires a functional UPR (Figure 6M). This suggests that an aberrant lipid composition can induce the UPR, which, in turn, is required for whorl formation. It is tempting to speculate as to whether whorl formation represents a quality control mechanism for sequestering aberrant membrane structures for subsequent degradation by an autophagy-like mechanism (Lingwood et al., 2009). Several questions remain; i.e., what initiates whorl formation, what stabilizes whorls, and what is their fate? Understanding these questions will help to establish the molecular mechanisms of lipid bilayer quality control complementing the well-known pathways of protein quality control.

Ubx2 Is a Linchpin for ER Homeostasis

This study uncovered cellular functions of Ubx2 in membrane homeostasis and ER bioactivity. Lack of Ubx2 resembles the loss of a linchpin and reveals intimately connected pathways as the underlying design principle of ER homeostasis. Instead of being autonomous processes, the ERAD, FA metabolism, membrane biogenesis, UPR, and ER morphology are interdependent and have evolved to communicate.

EXPERIMENTAL PROCEDURES

The strains and plasmids used in this study are listed in Table S4. The generation and analysis of the quantitative genetic interaction data with the E-MAP approach were carried out as previously described (Collins et al., 2010). The quantitation of lipids was performed essentially as described by Klose et al. (2012) with modifications from the original protocol (Ejsing et al., 2009). For electron microscopy studies, cells were cryoimmobilized by high-pressure freezing and after-freeze substitution in acetone stained with osmium tetroxide and uranyl acetate. Then, 70 nm sections were collected and contrasted with uranyl acetate. *OLE1* mRNA was quantitated relative to *ACT1* by quantitative PCR (qPCR) with standard techniques and a Power SYBR Green PCR Master Mix (Applied Biosystems). For more details, see the Supplemental Experimental Procedures.

Flow Cytometry Analysis

Cells were grown in yeast extract peptone dextrose (YPD) with additives as indicated from $OD_{600} = 0.1$ to $OD_{600} = 1$ and analyzed with a FACSCalibur flow cytometer (Becton Dickenson).

Immunoprecipitation

For IP experiments, 10 OD_{600} U of cells grown to $OD_{600} = 1$ were lysed in 1.4 ml IP buffer (25 mM Tris-HCl [pH 7.4], 150 mM NaCl, 2.5 mM $MgCl_2$, and 1% NP40 substitute) in the presence of 10 mM *N*-ethylmaleimide (NEM), 10 mM phenylmethanesulfonylfluoride, and a protease inhibitor cocktail (Roche) by vigorous shaking with zirconia beads for 10 min at 4°C. After 20 min at 4°C, the nonsolubilized material was removed by centrifugation (10,000 × *g* for 10 min) and precleared in presence of protein A beads. FLAG-tagged proteins were retrieved by 12 µl anti-FLAG M2 affinity gel (Sigma-Aldrich) and 3 hr of incubation at 4°C. After extensive washes with IP buffer, the immunoprecipitated proteins were eluted from the beads in sample buffer and analyzed by western blotting. For additional details, see the Supplemental Experimental Procedures.

Supplementary Material

Refer to Web version on PubMed Central for supplementary material.

Acknowledgments

REFERENCES

Aguilar PS, Fröhlich F, Rehman M, Shales M, Ulitsky I, Olivera-Couto A, Braberg H, Shamir R, Walter P, Mann M, et al. A plasma-membrane E-MAP reveals links of the eisosome with sphingolipid metabolism and endosomal trafficking. Nat. Struct. Mol. Biol. 2010; 17:901–908. [PubMed: 20526336]

Alberts SM, Sonntag C, Schäfer A, Wolf DH. Ubx4 modulates cdc48 activity and influences degradation of misfolded proteins of the endoplasmic reticulum. J. Biol. Chem. 2009; 284:16082–16089. [PubMed: 19359248]

Babu M, Vlasblom J, Pu S, Guo X, Graham C, Bean BD, Burston HE, Vizeacoumar FJ, Snider J, Phanse S, et al. Interaction landscape of membrane-protein complexes in Saccharomyces cerevisiae. Nature. 2012; 489:585–589. [PubMed: 22940862]

Bays NW, Gardner RG, Seelig LP, Joazeiro CA, Hampton RY. Hrd1p/Der3p is a membrane-anchored ubiquitin ligase required for ER-associated degradation. Nat. Cell Biol. 2001; 3:24–29. [PubMed: 11146622]

Beltrao P, Cagney G, Krogan NJ. Quantitative genetic interactions reveal biological modularity. Cell. 2010; 141:739–745. [PubMed: 20510918]

Bernales S, McDonald KL, Walter P. Autophagy counter-balances endoplasmic reticulum expansion during the unfolded protein response. PLoS Biol. 2006; 4:e423. [PubMed: 17132049]

Bordallo J, Plemper RK, Finger A, Wolf DH. Der3p/Hrd1p is required for endoplasmic reticulum-associated degradation of misfolded lumenal and integral membrane proteins. Mol. Biol. Cell. 1998; 9:209–222. [PubMed: 9437001]

Boumann HA, Gubbens J, Koorengevel MC, Oh CS, Martin CE, Heck AJ, Patton-Vogt J, Henry SA, de Kruijff B, de Kroon AI. Depletion of phosphatidylcholine in yeast induces shortening and increased saturation of the lipid acyl chains: evidence for regulation of intrinsic membrane curvature in a eukaryote. Mol. Biol. Cell. 2006; 17:1006–1017. [PubMed: 16339082]

Braun S, Matuschewski K, Rape M, Thoms S, Jentsch S. Role of the ubiquitin-selective CDC48(UFD1/NPL4)chaperone (segregase) in ERAD of OLE1 and other substrates. EMBO J. 2002; 21:615–621. [PubMed: 11847109]

Collins SR, Kemmeren P, Zhao XC, Greenblatt JF, Spencer F, Holstege FC, Weissman JS, Krogan NJ. Toward a comprehensive atlas of the physical interactome of Saccharomyces cerevisiae. Mol. Cell. Proteomics. 2007a; 6:439–450. [PubMed: 17200106]

Collins SR, Miller KM, Maas NL, Roguev A, Fillingham J, Chu CS, Schuldiner M, Gebbia M, Recht J, Shales M, et al. Functional dissection of protein complexes involved in yeast chromosome biology using a genetic interaction map. Nature. 2007b; 446:806–810. [PubMed: 17314980]

Collins SR, Roguev A, Krogan NJ. Quantitative genetic interaction mapping using the E-MAP approach. Methods Enzymol. 2010; 470:205–231. [PubMed: 20946812]

Costanzo M, Baryshnikova A, Bellay J, Kim Y, Spear ED, Sevier CS, Ding H, Koh JL, Toufighi K, Mostafavi S, et al. The genetic landscape of a cell. Science. 2010; 327:425–431. [PubMed: 20093466]

Deguil J, Pineau L, Rowland Snyder EC, Dupont S, Beney L, Gil A, Frapper G, Ferreira T. Modulation of lipid-induced ER stress by fatty acid shape. Traffic. 2011; 12:349–362. [PubMed: 21143717]

Eizirik DL, Cnop M. ER stress in pancreatic beta cells: the thin red line between adaptation and failure. Sci. Signal. 2010; 3:pe7. [PubMed: 20179270]

Ejsing CS, Sampaio JL, Surendranath V, Duchoslav E, Ekroos K, Klemm RW, Simons K, Shevchenko A. Global analysis of the yeast lipidome by quantitative shotgun mass spectrometry. Proc. Natl. Acad. Sci. USA. 2009; 106:2136–2141. [PubMed: 19174513]

Goder V, Carvalho P, Rapoport TA. The ER-associated degradation component Der1p and its homolog Dfm1p are contained in complexes with distinct cofactors of the ATPase Cdc48p. FEBS Lett. 2008; 582:1575–1580. [PubMed: 18407841]

Hampton RY, Gardner RG, Rine J. Role of 26S proteasome and HRD genes in the degradation of 3-hydroxy-3-methylglutaryl-CoA reductase, an integral endoplasmic reticulum membrane protein. Mol. Biol. Cell. 1996; 7:2029–2044. [PubMed: 8970163]

Han S, Lone MA, Schneiter R, Chang A. Orm1 and Orm2 are conserved endoplasmic reticulum membrane proteins regulating lipid homeostasis and protein quality control. Proc. Natl. Acad. Sci. USA. 2010; 107:5851–5856. [PubMed: 20212121]

Hapala I, Marza E, Ferreira T. Is fat so bad? Modulation of endoplasmic reticulum stress by lipid droplet formation. Biol. Cell. 2011; 103:271–285. [PubMed: 21729000]

Henry SA, Kohlwein SD, Carman GM. Metabolism and regulation of glycerolipids in the yeast Saccharomyces cerevisiae. Genetics. 2012; 190:317–349. [PubMed: 22345606]

Hitchcock AL, Krebber H, Frietze S, Lin A, Latterich M, Silver PA. The conserved npl4 protein complex mediates proteasome-dependent membrane-bound transcription factor activation. Mol. Biol. Cell. 2001; 12:3226–3241. [PubMed: 11598205]

Hoppe T, Matuschewski K, Rape M, Schlenker S, Ulrich HD, Jentsch S. Activation of a membrane-bound transcription factor by regulated ubiquitin/proteasome-dependent processing. Cell. 2000; 102:577–586. [PubMed: 11007476]

Hoppins S, Collins SR, Cassidy-Stone A, Hummel E, Devay RM, Lackner LL, Westermann B, Schuldiner M, Weissman JS, Nunnari J. A mitochondrial-focused genetic interaction map reveals a scaffold-like complex required for inner membrane organization in mitochondria. J. Cell Biol. 2011; 195:323–340. [PubMed: 21987634]

Jonikas MC, Collins SR, Denic V, Oh E, Quan EM, Schmid V, Weibezahn J, Schwappach B, Walter P, Weissman JS, Schuldiner M. Comprehensive characterization of genes required for protein folding in the endoplasmic reticulum. Science. 2009; 323:1693–1697. [PubMed: 19325107]

Kaiser HJ, Surma MA, Mayer F, Levental I, Grzybek M, Klemm RW, Da Cruz S, Meisinger C, Müller V, Simons K, Lingwood D. Molecular convergence of bacterial and eukaryotic surface order. J. Biol. Chem. 2011; 286:40631–40637. [PubMed: 21965671]

Kandasamy P, Vemula M, Oh CS, Chellappa R, Martin CE. Regulation of unsaturated fatty acid biosynthesis in Saccharomyces: the endoplasmic reticulum membrane protein, Mga2p, a

transcription activator of the OLE1 gene, regulates the stability of the OLE1 mRNA through exosome-mediated mechanisms. J. Biol. Chem. 2004; 279:36586–36592. [PubMed: 15220333]

Kim I, Xu W, Reed JC. Cell death and endoplasmic reticulum stress: disease relevance and therapeutic opportunities. Nat. Rev. Drug Discov. 2008; 7:1013–1030. [PubMed: 19043451]

Klose C, Ejsing CS, García-Sáez AJ, Kaiser HJ, Sampaio JL, Surma MA, Shevchenko A, Schwille P, Simons K. Yeast lipids can phase-separate into micrometer-scale membrane domains. J. Biol. Chem. 2010; 285:30224–30232. [PubMed: 20647309]

Klose C, Surma MA, Gerl MJ, Meyenhofer F, Shevchenko A, Simons K. Flexibility of a eukaryotic lipidome—insights from yeast lipidomics. PLoS ONE. 2012; 7:e35063. [PubMed: 22529973]

Kohlwein SD, Petschnigg J. SLipid-induced cell dysfunction and cell death: lessons from yeast. Curr. Hypertens. Rep. 2007; 9:455–461. [PubMed: 18367008]

Lee JN, Kim H, Yao H, Chen Y, Weng K, Ye J. Identification of Ubxd8 protein as a sensor for unsaturated fatty acids and regulator of triglyceride synthesis. Proc. Natl. Acad. Sci. USA. 2010; 107:21424–21429. [PubMed: 21115839]

Lingwood D, Schuck S, Ferguson C, Gerl M, Simons K. Morphological homeostasis by autophagy. Autophagy. 2009; 5:1039–1040. [PubMed: 19587538]

Lorch Y, Cairns BR, Zhang M, Kornberg RD. Activated RSC-nucleosome complex and persistently altered form of the nucleosome. Cell. 1998; 94:29–34. [PubMed: 9674424]

Martin CE, Oh CS, Jiang Y. Regulation of long chain unsaturated fatty acid synthesis in yeast. Biochim. Biophys. Acta. 2007; 1771:271–285. [PubMed: 16920014]

Neuber O, Jarosch E, Volkwein C, Walter J, Sommer T. Ubx2 links the Cdc48 complex to ER-associated protein degradation. Nat. Cell Biol. 2005; 7:993–998. [PubMed: 16179953]

Olzmann JA, Richter CM, Kopito RR. Spatial regulation of UBXD8 and p97/VCP controls ATGL-mediated lipid droplet turnover. Proc. Natl. Acad. Sci. USA. 2013; 110:1345–1350. [PubMed: 23297223]

Phillips R, Ursell T, Wiggins P, Sens P. Emerging roles for lipids in shaping membrane-protein function. Nature. 2009; 459:379–385. [PubMed: 19458714]

Pineau L, Colas J, Dupont S, Beney L, Fleurat-Lessard P, Berjeaud JM, Bergès T, Ferreira T. Lipid-induced ER stress: synergistic effects of sterols and saturated fatty acids. Traffic. 2009; 10:673–690. [PubMed: 19302420]

Promlek T, Ishiwata-Kimata Y, Shido M, Sakuramoto M, Kohno K, Kimata Y. Membrane aberrancy and unfolded proteins activate the endoplasmic reticulum stress sensor Ire1 in different ways. Mol. Biol. Cell. 2011; 22:3520–3532. [PubMed: 21775630]

Rape M, Hoppe T, Gorr I, Kalocay M, Richly H, Jentsch S. Mobilization of processed, membrane-tethered SPT23 transcription factor by CDC48(UFD1/NPL4), a ubiquitin-selective chaperone. Cell. 2001; 107:667–677. [PubMed: 11733065]

Roguev A, Bandyopadhyay S, Zofall M, Zhang K, Fischer T, Collins SR, Qu H, Shales M, Park HO, Hayles J, et al. Conservation and rewiring of functional modules revealed by an epistasis map in fission yeast. Science. 2008; 322:405–410. [PubMed: 18818364]

Ron D, Walter P. Signal integration in the endoplasmic reticulum unfolded protein response. Nat. Rev. Mol. Cell Biol. 2007; 8:519–529. [PubMed: 17565364]

Schuberth C, Buchberger A. Membrane-bound Ubx2 recruits Cdc48 to ubiquitin ligases and their substrates to ensure efficient ER-associated protein degradation. Nat. Cell Biol. 2005; 7:999–1006. [PubMed: 16179952]

Schuberth C, Buchberger A. UBX domain proteins: major regulators of the AAA ATPase Cdc48/p97. Cell. Mol. Life Sci. 2008; 65:2360–2371. [PubMed: 18438607]

Schuck S, Prinz WA, Thorn KS, Voss C, Walter P. Membrane expansion alleviates endoplasmic reticulum stress independently of the unfolded protein response. J. Cell Biol. 2009; 187:525–536. [PubMed: 19948500]

Schuldiner M, Collins SR, Thompson NJ, Denic V, Bhamidipati A, Punna T, Ihmels J, Andrews B, Boone C, Greenblatt JF, et al. Exploration of the function and organization of the yeast early secretory pathway through an epistatic miniarray profile. Cell. 2005; 123:507–519. [PubMed: 16269340]

Shcherbik N, Haines DS. Cdc48p(Npl4p/Ufd1p) binds and segregates membrane-anchored/tethered complexes via a polyubiquitin signal present on the anchors. Mol. Cell. 2007; 25:385–397. [PubMed: 17289586]

Shcherbik N, Zoladek T, Nickels JT, Haines DS. Rsp5p is required for ER bound Mga2p120 polyubiquitination and release of the processed/tethered transactivator Mga2p90. Curr. Biol. 2003; 13:1227–1233. [PubMed: 12867034]

Snapp EL, Hegde RS, Francolini M, Lombardo F, Colombo S, Pedrazzini E, Borgese N, Lippincott-Schwartz J. Formation of stacked ER cisternae by low affinity protein interactions. J. Cell Biol. 2003; 163:257–269. [PubMed: 14581454]

Stukey JE, McDonough VM, Martin CE. The OLE1 gene of Saccharomyces cerevisiae encodes the delta 9 fatty acid desaturase and can be functionally replaced by the rat stearoyl-CoA desaturase gene. J. Biol. Chem. 1990; 265:20144–20149. [PubMed: 1978720]

Thibault G, Ismail N, Ng DT. The unfolded protein response supports cellular robustness as a broad-spectrum compensatory pathway. Proc. Natl. Acad. Sci. USA. 2011; 108:20597–20602. [PubMed: 22143797]

Thibault G, Shui G, Kim W, McAlister GC, Ismail N, Gygi SP, Wenk MR, Ng DT. The membrane stress response buffers lethal effects of lipid disequilibrium by reprogramming the protein homeostasis network. Mol. Cell. 2012; 48:16–27. [PubMed: 23000174]

van Meer G, Voelker DR, Feigenson GW. Membrane lipids: where they are and how they behave. Nat. Rev. Mol. Cell Biol. 2008; 9:112–124. [PubMed: 18216768]

Vembar SS, Brodsky JL. One step at a time: endoplasmic reticulum-associated degradation. Nat. Rev. Mol. Cell Biol. 2008; 9:944–957. [PubMed: 19002207]

Voeltz GK, Rolls MM, Rapoport TA. Structural organization of the endoplasmic reticulum. EMBO Rep. 2002; 3:944–950. [PubMed: 12370207]

Volmer R, van der Ploeg K, Ron D. Membrane lipid saturation activates endoplasmic reticulum unfolded protein response transducers through their transmembrane domains. Proc. Natl. Acad. Sci. USA. 2013; 110:4628–4633. [PubMed: 23487760]

Wang CW, Lee SC. The ubiquitin-like (UBX)-domain-containing protein Ubx2/Ubxd8 regulates lipid droplet homeostasis. J. Cell Sci. 2012; 125:2930–2939. [PubMed: 22454508]

Wilmes GM, Bergkessel M, Bandyopadhyay S, Shales M, Braberg H, Cagney G, Collins SR, Whitworth GB, Kress TL, Weissman JS, et al. A genetic interaction map of RNA-processing factors reveals links between Sem1/Dss1-containing complexes and mRNA export and splicing. Mol. Cell. 2008; 32:735–746. [PubMed: 19061648]
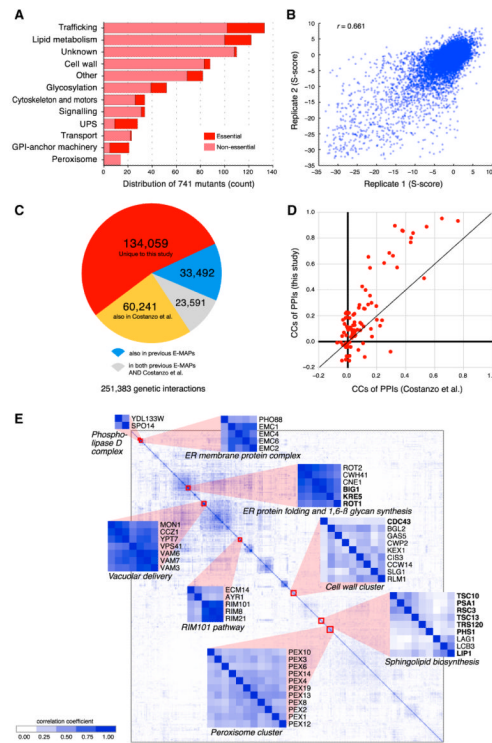
Figure 1. Overview of the E-MAP

(A) The functional composition of the lipid E-MAP. Light and dark red indicate nonessential and essential genes, respectively.

(B) A scatter plot of the replicate scores (i.e., A-B versus B-A pairs).

(C) A comparison of the genetic interactions identified in this work and in other E-MAPs and a more global analysis (see Figure S1 for details).

(D) The correlation of genetic interaction profiles from this study and the Costanzo et al. (2010) data set focusing on genes whose proteins participate in protein-protein interactions.

(E) Hierarchical clustering of the correlation of genetic interaction profiles for each pair of genes from the lipid E-MAP. Negative correlations were included for clustering but have been mapped to zero in the clustergram. Essential genes are indicated in bold.
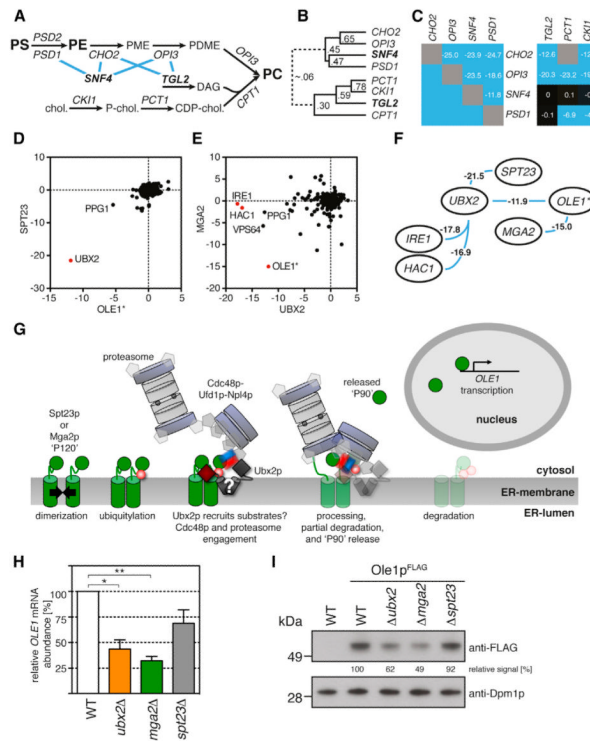
Figure 2. Genetic Interactions Assign Gene Functions to Specific Lipid Metabolic Pathways
(A) A schematic diagram of the of the PC synthesis pathway. The PS conversion is depicted on the top, and the de novo synthesis (Kennedy pathway) is depicted on the bottom. Blue lines indicate negative genetic interactions.

(B) Clustering of genetic interaction profiles for *SNF4*, *TGL2*, and PC-synthesis-related genes. Numbers are correlation coefficients. The dotted connection indicates a very weak correlation.

(C) The genetic interaction scores of PC-synthesis-related genes with *SNF4* and *TGL2*. Blue indicates GI scores < -2.5. Gray indicates unavailable data.

(D and E) Scatter plots of genetic interaction scores between the indicated genes and all other genes of the E-MAP. Data points discussed in the text are highlighted red.

(F) Genetic interactions of *UBX2* highlight the crosstalk of the UPR (*IRE1* and *HAC1*), the ERAD machinery (*UBX2*), and FA metabolism (*SPT23*, *MGA2*, and *OLE1*). *OLE1*, an essential gene, was present as a DAmP allele (*) (Schuldiner et al., 2005). Only significant interactions are shown.

(G) A schematic model of the OLE pathway.

(H) The relative *OLE1* mRNA levels of the indicated cells were determined by qPCR. Data are represented as mean ± SD. The *OLE1* mRNA level relative to actin of mutant cells was compared to the WT level. Results of an unpaired, two-tailed t test for the genotype are shown. *$p < 0.05$; **$p < 0.01$ (n = 3).

(I) WT cells and deletants with and without genomically FLAG-tagged Ole1 were grown in YPD to $OD_{600} = 1$. Cell lysates were immunoblotted as indicated, and the relative signal was determined by densitometry.
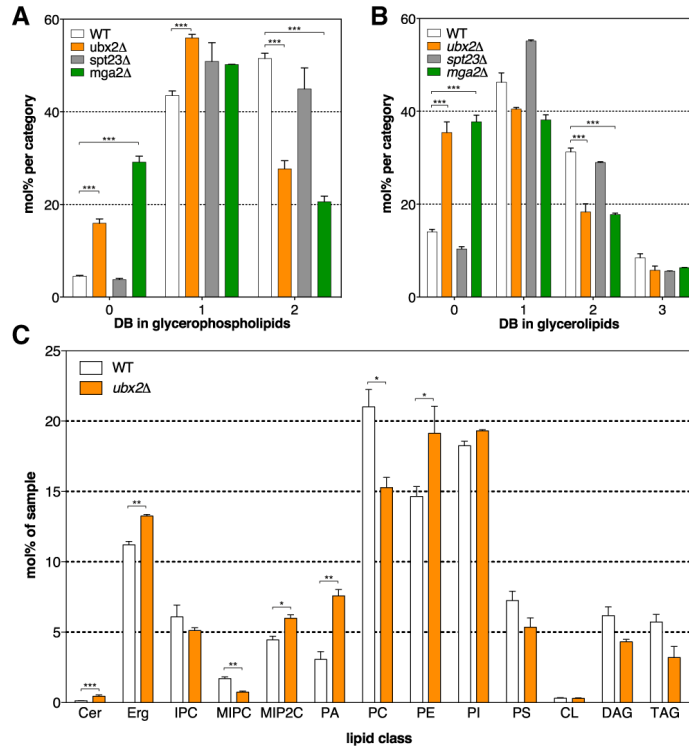
Figure 3. *UBX2* Is Involved in Lipid Metabolism

Lipidomes of the analyzed mutants are shown.

(A) Total double bonds (DB) of glycerophospholipids (GP; cardiolipin omitted for clarity), given as the sum of DB in FAs, in mol% of all glycerophospholipids.

(B) Total DB of glycerolipids (GL; DAG and TAG), given as the sum of DB in FAs, in mol % of all glycerolipids.

(A and B) Highly significant deviations from WT cells. ***$p < 0.001$ in an unpaired, two-tailed t test (n = 6 for WT and n = 2 for *ubx2* and *mga2*).

(C) Lipid class composition in mol% of total lipids in the sample. *$p < 0.05$; **$p < 0.01$; ***$p < 0.001$ in an unpaired, two-tailed t test (n = 6 for WT and n = 2 for *ubx2* and *mga2*).

Data are represented as mean ± SD. More data from lipid analyses are provided in Figures S2–S4 and Table S3.
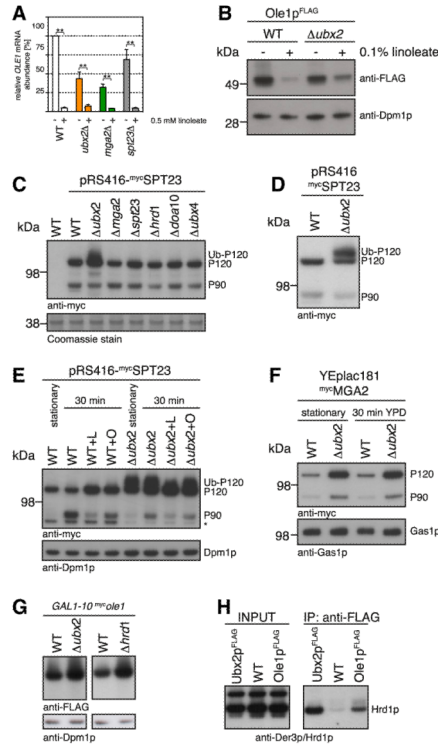
Figure 4. *UBX2* Modulates the Ole1 Level by Distinct Mechanisms
(A) The relative mRNA was determined as in Figure 2I. If indicated, the medium was supplemented with 0.5 mM linoleate (UFA). *p < 0.05; **p < 0.01 (unpaired, two-tailed t test; n = 3). Data are represented as mean ± SD.
(B) WT cells and deletants with and without genomically FLAG-tagged Ole1 were grown in YPD to $OD_{600} = 1$. Where indicated, the medium contained 0.1% linoleate. Cell lysates were immunoblotted as indicated.
(C–E) WT cells and deletants with and without N-terminally Myc-tagged Spt23 expressed from its endogenous promoter on a plasmid were grown in YPD to $OD_{600} = 1$ (C and D) or for the indicated times in YPD with and without sodium linoleate (+L, 0.1%) or sodium oleate (+O, 0.1%). Cell lysates were immunoblotted as indicated.
(F) WT and *ubx2* cells carrying a plasmid encoding N-terminally Myc-tagged Mga2 were grown in synthetic complete dropout medium without leucine. The asterisk indicates an unspecific signal that is consistently higher in WT cells in comparison to *ubx2* cells.
(G) Catalytically inactive 3× Myc-tagged Ole1 was expressed from a GAL promoter in YPD with galactose. Cell lysates were immunoblotted as indicated.
(H) Lysates of cells expressing genomically tagged Ubx2-FLAG and Ole1-FLAG were subjected to IP. Coprecipitated material was immunoblotted as indicated. NEM was present in the lysis buffer in order to prevent the deubiquitylation of Ole1. Cell lysates were equally loaded with WT cells as a specificity control.
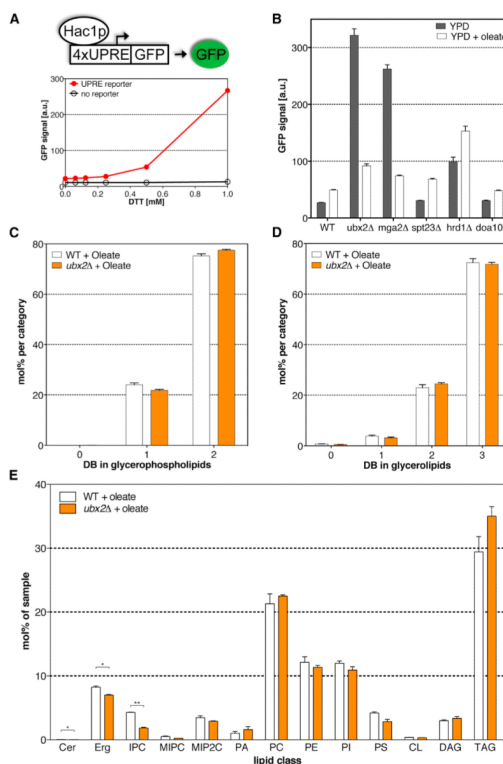
Figure 5. Misregulated FA Desaturation Induces the UPR and Can Be Reversed by Exogenous UFAs

(A) Quantifying UPR levels in yeast with a GFP reporter as a function of DTT concentration with FACS. Cells without reporter constructs served as a control.

(B) The UPR reporter level in deletants exponentially grown in YPD (gray) and in the presence of 0.01% oleate (white).

(C and D) WT cells and deletants grown to $OD_{600} = 1$ in YPD with 0.15% Brij35 and 0.1% sodium oleate at 30°C.

(C) Total DB of glycerophospholipids (GP; cardiolipin omitted for clarity), given as the sum of DB in FAs, in mol% of all glycerophospholipids.

(D) Total DB of glycerolipids (GL; DAG and TAG), given as the sum of DB in FAs, in mol% of all glycerolipids.

(E) Lipid class composition in mol% of total lipids in the sample. $*p < 0.05$; $**p < 0.01$; $***p < 0.001$ (unpaired, two-tailed t test; $n = 2$).

(B–E) Data are represented as mean ± SD.
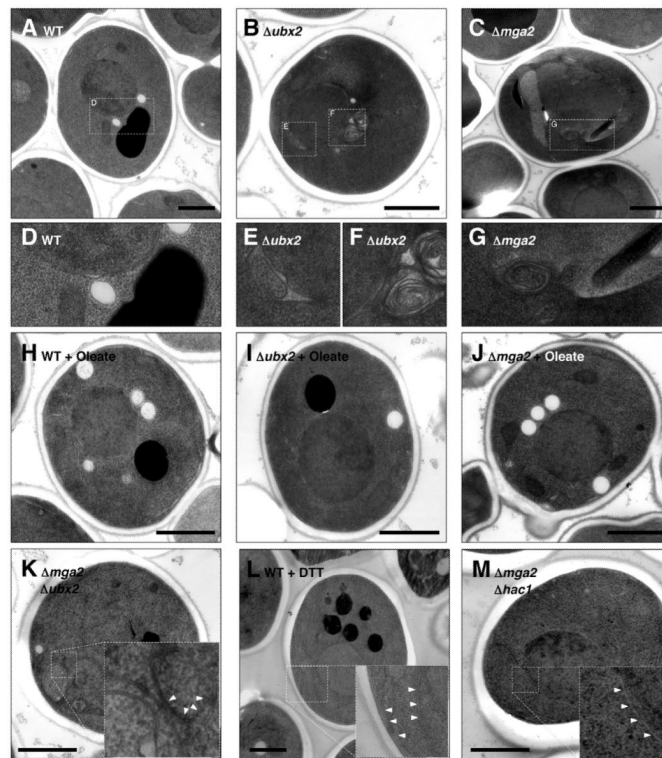
Figure 6. Misregulated FA Desaturation Induces the Expansion of the Outer Nuclear Membrane and the Formation of ER Whorls

(A–M) Electron micrographs of WT cells and deletants harvested at $OD_{600} = 3$.

(A–G, K, and M) Cells grown in YPD.

(H–J) Cells grown in YPD with 0.15% Brij35 and 0.1% oleate.

(L) WT cells grown in YPD and stressed by a 2 hr treatment with 8 mM DTT prior to harvesting.

(K–M) The white arrows indicate the ER.

(A–C) and (H–M) The scale bar represents 1 μm.